JOURNAL OF SOLID STATE CHEMISTRY 26, 1–16 (1978)

# Microsyntactic Intergrowth and Defects in Barium Ferrite Compounds*

Y. HIROTSU† AND H. SATO

*School of Materials Engineering, Purdue University, West Lafayette, Indiana 47907*

Received November 4, 1977; in final form February 2, 1978

The structural characteristics and defects of barium ferrite compounds in the composition range along the line which connects the composition of the $M$ compound ($BaFe_{12}O_{19}$) and that of the $W$ compound ($BaFe_{18}O_{27}$) were investigated by transmission electron microscopy. An intergrowth of several different compounds was found to occur in a microsyntactic fashion similar to that observed previously in Mg-doped $\beta$-alumina. The characteristics of both the intergrowth and the defects are discussed relative to independent structural subunit blocks $R$ and $S$ in these compounds. Also, the significance of microsyntactic intergrowth to $\beta$-alumina type compounds is discussed.

## Introduction

The interest of the present work has stemmed from our previous observation of $\beta$-alumina type compounds by transmission electron microscopy (*1*). Lattice imaging of Mg-doped $\beta$-alumina revealed that structures of the same symmetry but of different unit cell sizes intergrew in a syntactic fashion on a unit cell scale (*1*, *2*). This intergrowth gave the appearance that the crystalline repeat distance in the $c$-direction of this compound was nonuniform. This feature was interpreted as a syntactic intergrowth of $\beta$-alumina type compounds $D(nS)D^*(nS^*)$ ($n = 0, 1, 2, \ldots$) in terms of structural subunit blocks $D$ and $S$ on a unit cell scale.[1] $D^*$ and $S^*$ are the same as $D$ and $S$, respectively, but are rotated by 180° with respect to $D$ and $S$ around the $c$-axis. $S$ is called the spinel block and is the structural unit of the spinel structure, while $D$ is called the defect block which is composed of a "defect layer" including $Na^+$ ions and two flanking closed packed oxygen layers. The syntactic intergrowth on a unit cell scale will be called the microsyntactic intergrowth although one of the present authors used the same expression for syntactic intergrowth of different polytypes of SiC in extremely narrow alternating bands earlier (*3*). Syntactic intergrowth of $\beta$- and $\beta''$-alumina (*4*) also occurs in a similar fashion (*1*).

The most interesting feature of the microsyntactic intergrowth in $\beta$-alumina type compounds is that both the structural subunit blocks $D$ and $S$ behave as if they were independent structural units (*1*). If this is true, it would be possible to synthesize a particular type of $\beta$-alumina type compounds with a higher density of conducting layers (compound $DD^*$ for example) which may be a substance of higher ionic conductivity. Further, it indicates that both $D$ and $S$ are in

* The work was supported in part by the National Science Foundation Grant DMR7502959 and MRL Program DMR7203018A04.

† On leave of absence from Tokyo Institute of Technology, Oh-okayama, Meguro-ku, Tokyo.

[1] The existence of only two ($n = 1$: $\beta$-alumina and $n = 2$: $\beta'''$-alumina (*5*)) of $\beta$-alumina type compounds has been reported.



0022-4596/78/0261/0001$02.00/0

principle charge-compensated individually (*1*). The interpretation of "nonstoichiometry" of $\beta$-alumina (*6–11*) should also take this situation into account.

Ba-ferrite ($BaOFe_{12}O_{18}$) is isomorphous with $\beta$-alumina except for the difference in the valences of Ba and Na and hence in the structure of the "defect layer" (*12–14*). The "nonstoichiometry" in the Ba content in the defect layer, however, has not been noted (*14–16*). A series of compounds are known in the BaO–*Me*O–$Fe_2O_3$ system where *Me* stands for divalent Fe series transition metal elements and a similar block concept has long been used in the description of these compounds (*14, 15*). The observation of syntactic intergrowth of several compounds in this system has also been reported (*17–19*). Further, a compound which corresponds to *DD** has been synthesized by the addition of Ti in this system (*20*). Therefore, because of these similarities in the structure and differences concerning the stoichiometry as well as the difference concerning the ionicity of Fe and Al in forming the spinel structure, it seems worthwhile to investigate the relationships of these two types of compounds with respect to the microsyntactic intergrowth.

### *Structural Subunit Blocks in Ba-Ferrites*

Before presenting our experimental results on Ba-ferrites, a brief explanation of the block concept commonly adopted in describing these compounds which appear in the BaO–*Me*O–$Fe_2O_3$ system will be appropriate.

Braun first applied the block concept extensively in describing a series of structures in this system (*14*) and this description was further reorganized by Smit and Wijn (*15*). Kohn and Eckart have extended this work in analyzing a number of long period structures with X rays (*21–23*). These results are summarized in Figs. 1 and 2. Figure 1 shows the unit cells of various structures in terms of the block concept and Fig. 2 shows the locations of these compounds in the composition diagram.

In Fig. 1, *M* ($=BaFe_{12}O_{19}$, Ba-ferrite) and

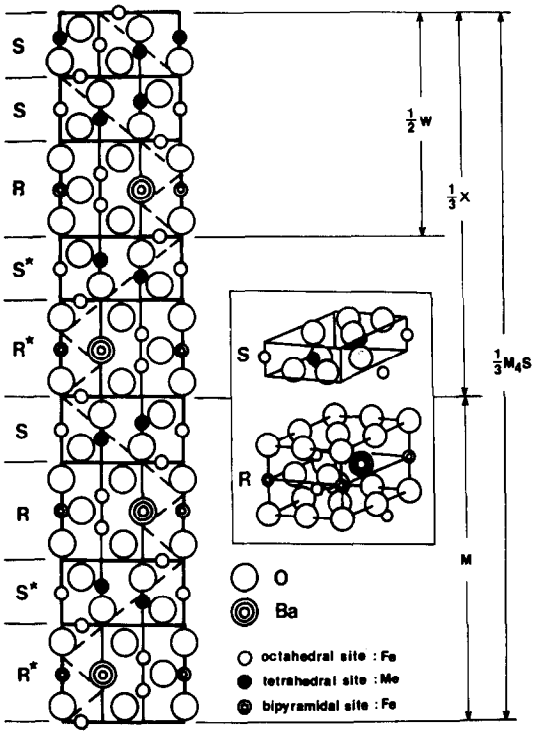


FIG. 1. Structures of barium ferrite compounds in terms of structural subunit blocks, *R* and *S*. *R** and *S** are the same as *R* and *S*, respectively, but are rotated by 180° with respect to the *c*-axis.

*W* ($=BaFe_2^{II}Fe_{16}^{III}O_{27}$) have hexagonal symmetry and are described in terms of structural subunit blocks *R* and *S* as *RSR*S** and

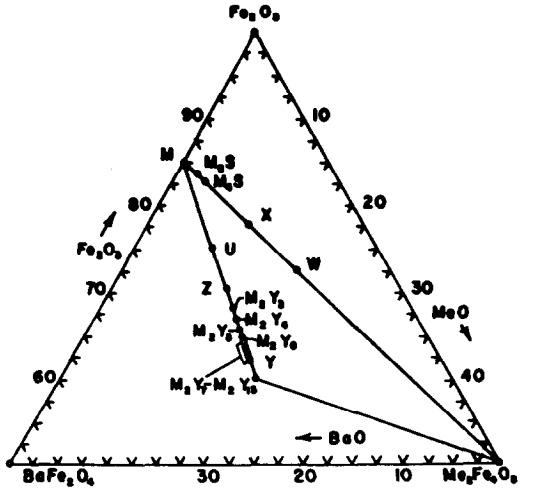


FIG. 2. Composition diagram showing barium ferrite compounds.

*RSSR*S*S**, respectively. *R* corresponds to *D* for $\beta$-alumina and hence *M* and *W* are isomorphous with $\beta$- and $\beta'''$-alumina, respectively. The *S* block is again the unit building block of the spinel structure but is composed of ferrite instead of aluminate. *X* and $M_4S$, on the other hand, have rhombohedral symmetry and only one third of their unit cells are indicated in Fig. 1. Since the Ba content in the *R* block is assumed to be a constant, the Ba content in the above-mentioned compounds is determined by the number of *R* blocks in the structural units. The composition of these compounds is indicated in the phase diagram (Fig. 2).

*Experimental Results*

Since the purpose of this work is to compare barium ferrite compounds with $\beta$-alumina, we are mostly interested in the compounds in the composition range between *M* and *W*. (See Fig. 2.) Six specimens which correspond to compositions *M*, *X*, and *W* and three others between $M_6S$–$M_4S$, $M_4S$–*X*, and *X*–*W* were prepared. These specimens were made by mixing $BaCO_3$, $\alpha$-$Fe_2O_3$ and FeO powder in the proper amounts and then melting the mixtures at 1500°C in air. For electron microscope observations, specimens were finely crushed and the powders were mounted on carbon-coated copper grids. Siemens Elmiskop I and Hitachi–11A electron microscopes were used for this purpose. We also used a JEM 100–B electron microscope at Northwestern University for work which required higher resolution.

To minimize radiation damage, the beam current in the electron microscopes was always kept bleow 10 $\mu$A with a condenser aperture as large as 400 $\mu$m and long time observation of the same area was avoided. It was found that barium ferrite compounds were far more resistant to radiation damage than $\beta$-alumina type compounds and, hence, the observation of these compounds was found to be much easier.

Identification of each compound was easily made by analysis of the selected area diffraction pattern with either the (*hk*.0) or the (*h*0.0) plane perpendicular to the incident beam based on the reported crystal data for each compound. (See Table I.)

For bright field lattice imaging, strongly excited reflections in the (00.*l*) row along with the central beam were used while in the case of dark field imaging, strong reflections in the rows of (00.*l*) or (*h*0.*l*) were used. Also, for both the Siemens and the Hitachi electron microscopes, objective apertures of 20 $\mu$m in diameter were used which corresponded approximately to a 0.2-$Å^{-1}$-diameter area in the diffraction patterns.

TABLE I

SPECIFICATION OF COMPOUNDS WHICH APPEAR ALONG THE COMPOSITION LINE CONNECTING THE *M* AND THE *W* COMPOUNDS

| Ideal Stoichiometry | Symbol | Structure | C(Å) | Space Group |
|---|---|---|---|---|
| $BaFe_{12}O_{19}$ (M) | 10H | 113113 | 23.20 | $P6_3/mmc$ |
| $BaMe_2Fe_{16}O_{27}$ (W,MS) | 14H | 115115 | 32.84 | $P6_3/mmc$ |
| $Ba_2Me_2Fe_{28}O_{46}$ ($X$,$M_2S$) | 36R | $(113115)_3$ | 84.11 | $R\bar{3}m$ |
| $Ba_4Me_2Fe_{52}O_{84}$ ($M_4S$) | 66R | $[(113)_3115]_3$ | 153.85 | $R\bar{3}m$ |
| $Ba_6Me_2Fe_{76}O_{122}$ ($M_6S$) | 96R | $[(113)_5115]_3$ | 223.40 | $R\bar{3}m$ |

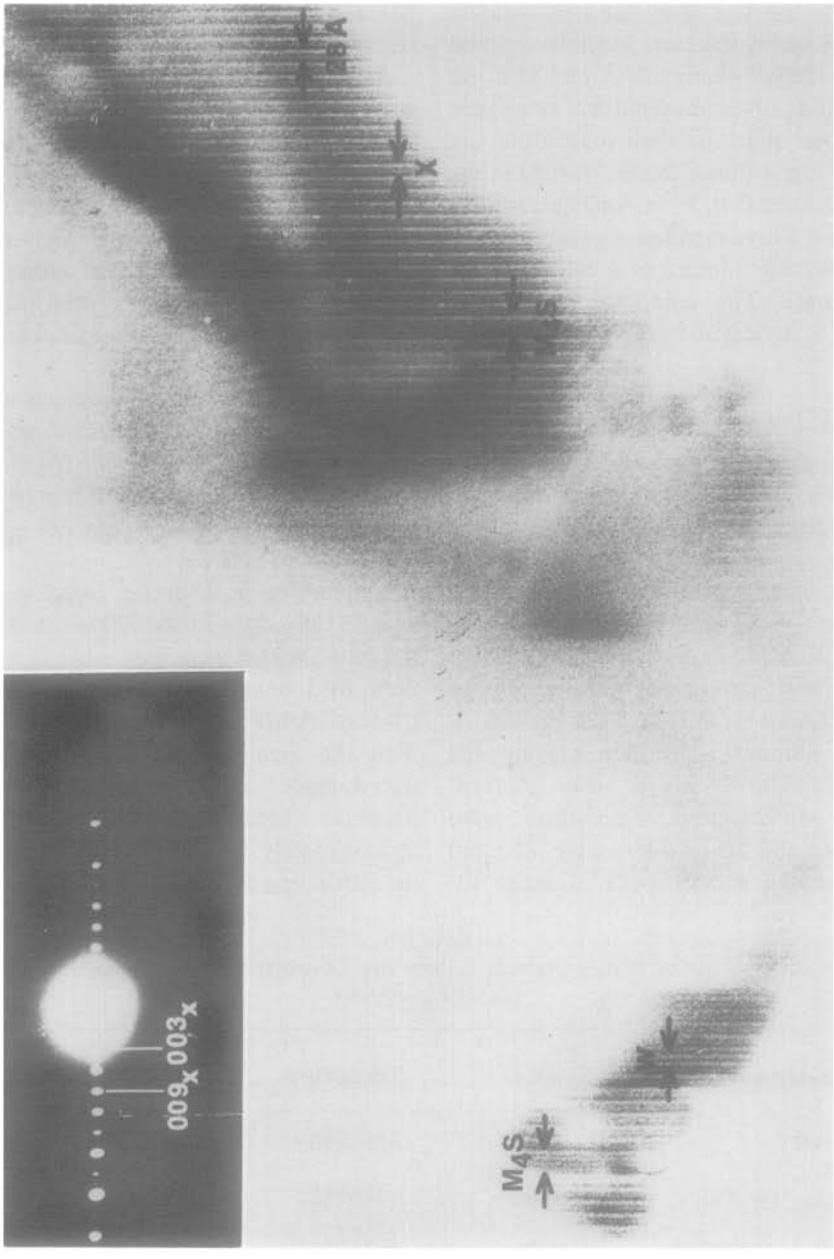


FIG. 3. Microsyntactic growth of the $M_4S$ and the $W$ compound in the $X$ compound with a corresponding selected area diffraction pattern.

In all specimens investigated, an intergrowth of a variety of structures in a microsyntactic fashion very similar to that in $\beta$-alumina was found. Also, a variety of defects which were characteristic of long period structures was observed. Typical examples with analyses will be presented in the following.

*Microsyntactic Intergrowth*

The microsyntactic intergrowth was found primarily in the specimens which corresponded to the composition $M$, $M_4S$–$M_6S$ and $X$–$M_4S$. Irrespective of the composition of the specimens, the $W$ compound was usually observed as a component in these mixed period structures.

Figure 3 shows an example of the existence of mixed periods in the matrix of the $X$-structure. The existence of isolated single unit cell periods of the $W$ and $M_4S$ structures in the $X$ matrix is clearly recognized as stripes of widths 33 and 51 Å, respectively. For $M_4S$, the width (51 Å) corresponds to one third of the unit crystallographic structure generally taken ($c$ = 153.8 Å). In fact, 51Å is the width of $4M + S$ and is the unit physical repeat

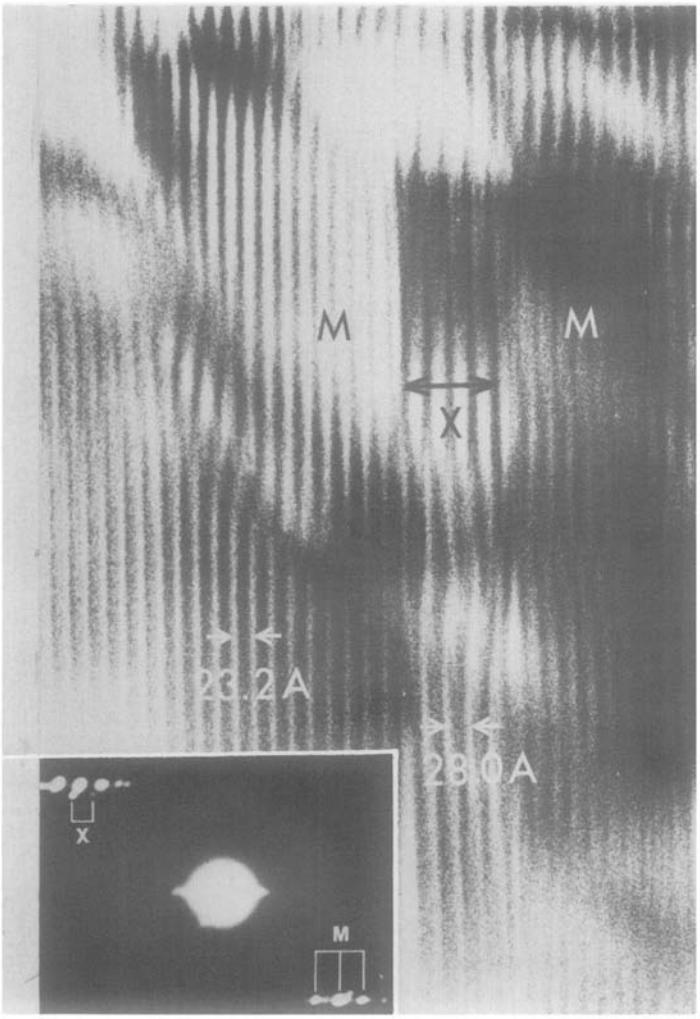


FIG. 4. Microsyntactic growth of the $X$ structure in the $M$ compound with corresponding selected area diffraction pattern. $X$ and $M$ in the diffraction pattern represent the diffraction spots of the $X$ and $M$ structure, respectively.

distance for the rhombohedral $M_4S$ structure. The image of the $W$ structure (33 Å) is a double width image, created by a double diffraction since the double diffraction spot is utilized to form this image. Such line images created by a double diffraction are referred to simply as double width images in this paper.

Figure 4 shows an example of a syntactic intergrowth of the $X$ structure in the matrix of the $M$ structure. The stripes of 23 Å for $M$ are again a double width image from double diffraction. Here, a narrow band of the $X$ structure with the stripe width of 28 Å is observed in a syntactic fashion in the matrix of the $M$ structure. A disturbance in the stripe patterns observed in the image can be due either to a strain created by underlying dislocations which are observed indirectly here

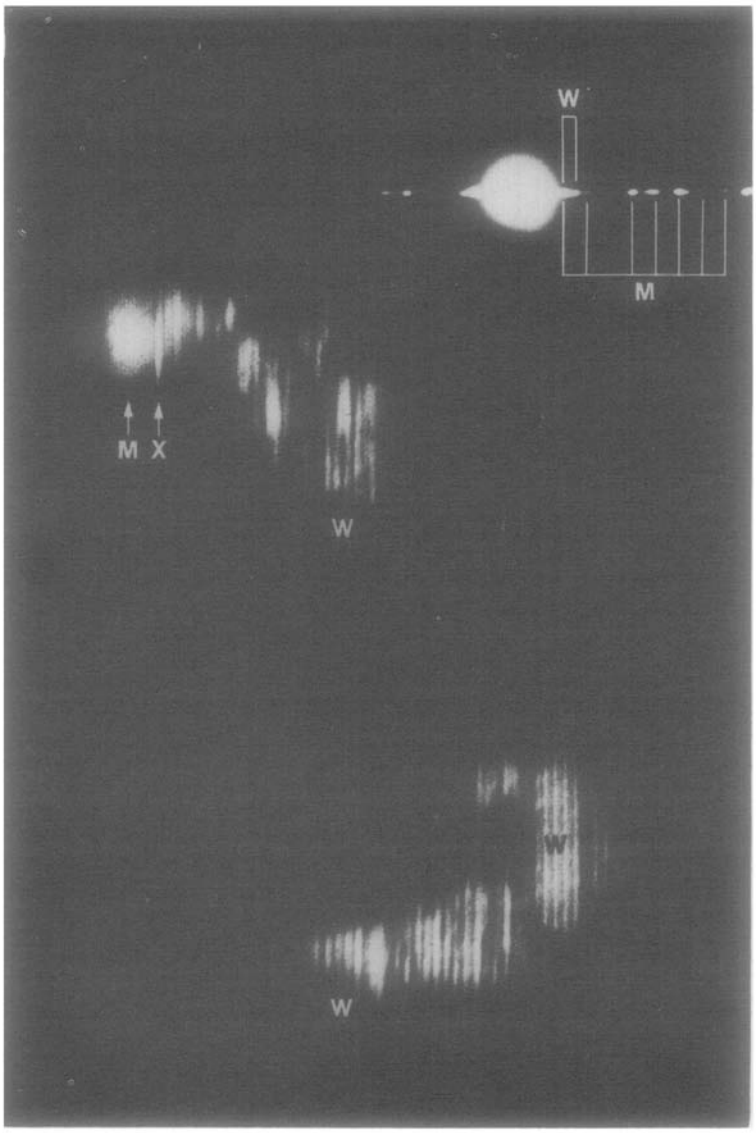


FIG. 5. Darkfield image of the microsyntactic growth of $M$ and $X$ in $W$. The picture was taken by using the first several spots along the [00.1] reciprocal lattice direction of the diffraction pattern shown.

as double width images or to a local thickness change of the specimen. The selected area diffraction pattern in the inset shows, however, that the rows of diffraction spots from the $X$ structure are not parallel to those of the $M$ structure. This is interpreted to be due to the lattice strain created by the dislocation.

A dark field image of the microsyntactic coexistence of the $M$, $X$, and $W$ structures is shown in Fig. 5. This was taken by using several reflections next to the origin (but excluding the origin) along the [00.1] direction in the reciprocal lattice as shown in the inset. In the matrix of $M$ with 12-Å stripe width, isolated unit cells of $X$ with 28-Å stripe width are observed. The highly strained image corresponds to the existence of the diffuse streaks around the diffraction spots in the inset.

Figure 6 shows an example in which different structures coexist in a random fashion. In the middle part of the figure, both the $X$ and the $W$ structures are observed as a random mixture. The $M_4S$ and the $M_5S$ structures are also observed among them.

*Defects*

A microsyntactic intergrowth of various compounds is a kind of defect related to the structural subunit blocks. If such structural subunit blocks are really basic structural units of this type of compound, the structure of more familiar defects like dislocations which can be related to the (00.1) planes should also reflect the same feature. We have observed several types of defects of this sort. Typical examples of such defects are described below to clarify the block concept further.

In order to obtain direct information concerning defects, the crystals have to be tilted so that double diffracted beams (00.±1), (00.±3), . . . of the $M$ and the $W$ compounds are eliminated from the image formation. If such double diffracted beams are used, images

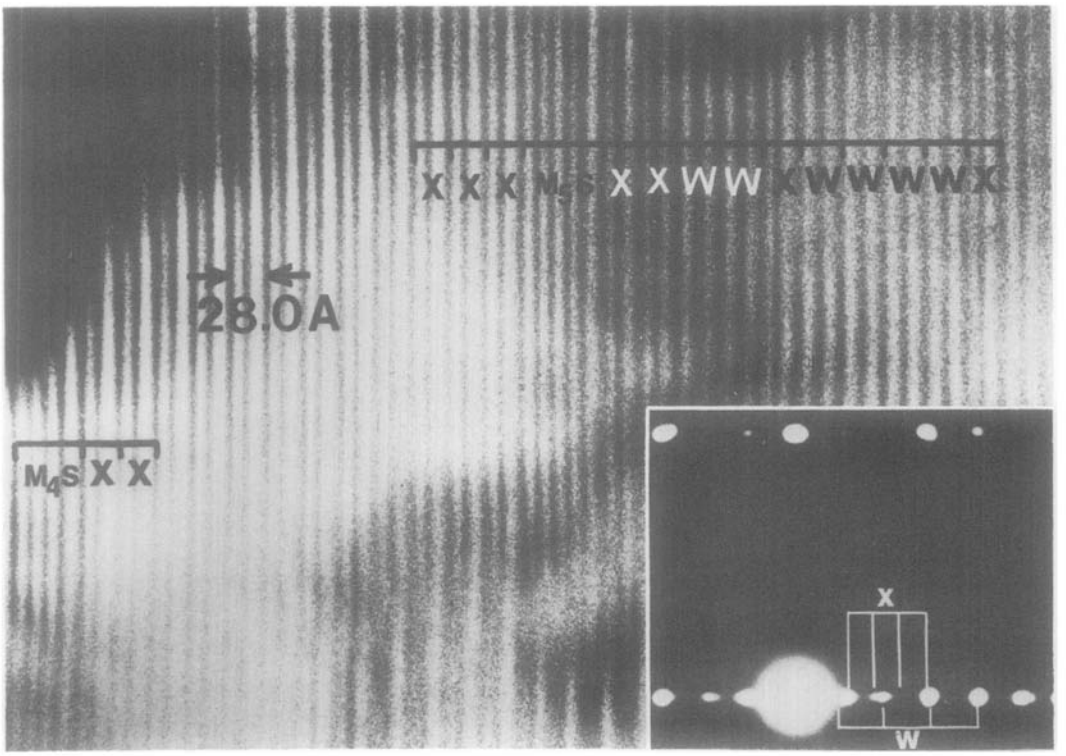


FIG. 6. Randomly mixed $X$, $W$, $M_5S$ compounds with a corresponding selected area diffraction pattern.

observed are double width fringes created by the superposition of two lattice planes and only indirect information of defects which are related to planes other than (00.1) is obtained. Such indirect information due to double width images should carefully be selected.

Figure 7 shows the lattice image which was taken under an illumination condition such that double diffraction spots in the (00.*l*) series derived from the *M* structure were weak. In this case, an 11.6-Å lattice image which corresponds to that of the (00.2) planes of the *M* structure is observed. At some places such as in the areas along the lines A–B and C–D, however, stripe widths which are smaller than 11.6 Å can be observed. Figure 8 shows such stripes in the microdensitometer profiles along the line A–B (indicated by *a*) and C–D (indicated by *b*). The widths *a* and *b* are about 6.7 and 4.5 Å and correspond to the widths of the *R* and the *S* blocks, respectively. It should be noted that the isolated existence of the *R* and the *S* blocks is equivalent to the microsyntactic intergrowth of several kinds of compounds.

In both the *M* and the *W* structures, images of pure edge dislocations with a Burgers vector $1/2c$, where $c$ is the lattice vector in the $c$-

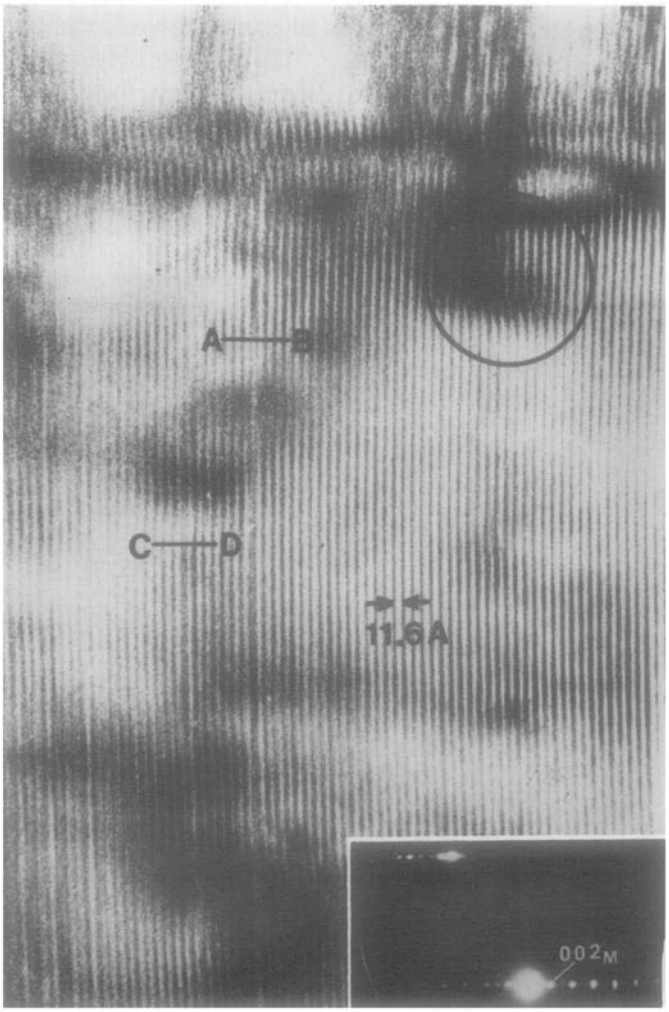


FIG. 7. Lattice image of the *M* compound with defects with a corresponding diffraction pattern.

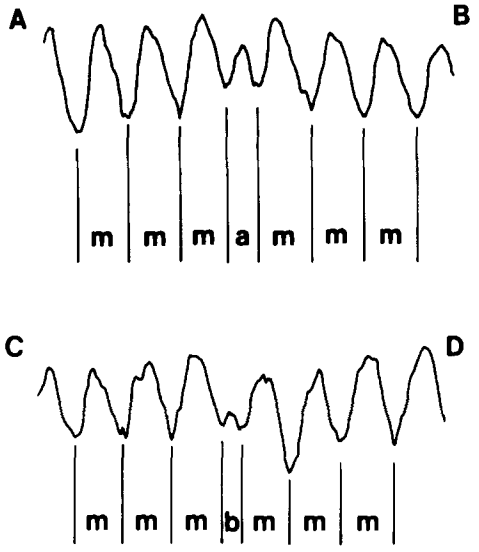


FIG. 8. Microdensitometer profile along lines A–B and C–D in Fig. 7. The widths of stripes *a* and *b* correspond to 6.7 and 4.5 Å, respectively.

direction, are often found. These are similar to those often found in $\beta$-alumina. An example is found in the encircled area in Fig. 7. The area includes a pair of edge dislocations and the image is shown enlarged in Fig. 9. The locations of the two dislocation cores are shown by arrows. Since half of the unit cell is missing along the (00.1) plane, the remaining half of the unit cell can only match with the other parts of the crystal across the antiphase boundaries. Two possible models for such antiphase boundary formation are shown schematically in Fig. 9. The necessity for the existence of antiphase boundaries is a source of extra energy involved in the dislocation formation. Between the two possible models shown in Fig. 9, the structure with the limited antiphase boundary connecting the two cores (a) seems to be more favorable.

The existence of dislocations with such a large Burgers vector should be accompanied by a large elastic strain which is proportional to the square of the Burgers vector. In Fig. 9, two dislocations of different signs form as a pair which seems to relax the stored elastic energy created by the dislocations. Nevertheless, the frequent existence of dislocations with such a large Burgers vector (corresponding to sizes of subunit blocks) is a further indication of the stability of such subunit blocks and hence, the possible charge neutrality of these blocks.

The appearance of apparent mixed periods in lattice images is not always a proof of the microsyntactic intergrowth. They are often

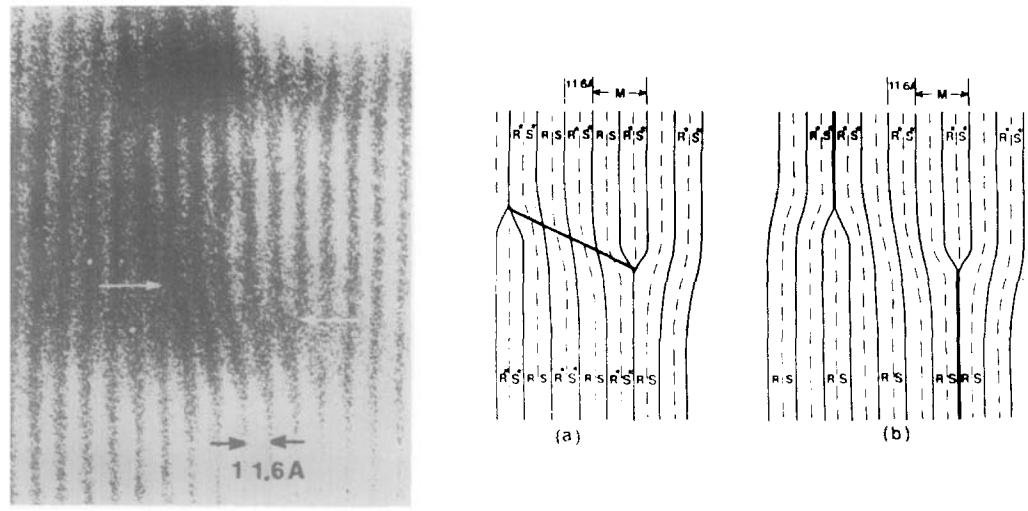


FIG. 9. Enlarged image of a pair of dislocations which appear in the circle of Fig. 7. Arrows show the positions of the dislocation cores. (a) and (b) are two possible structural models of the dislocations.

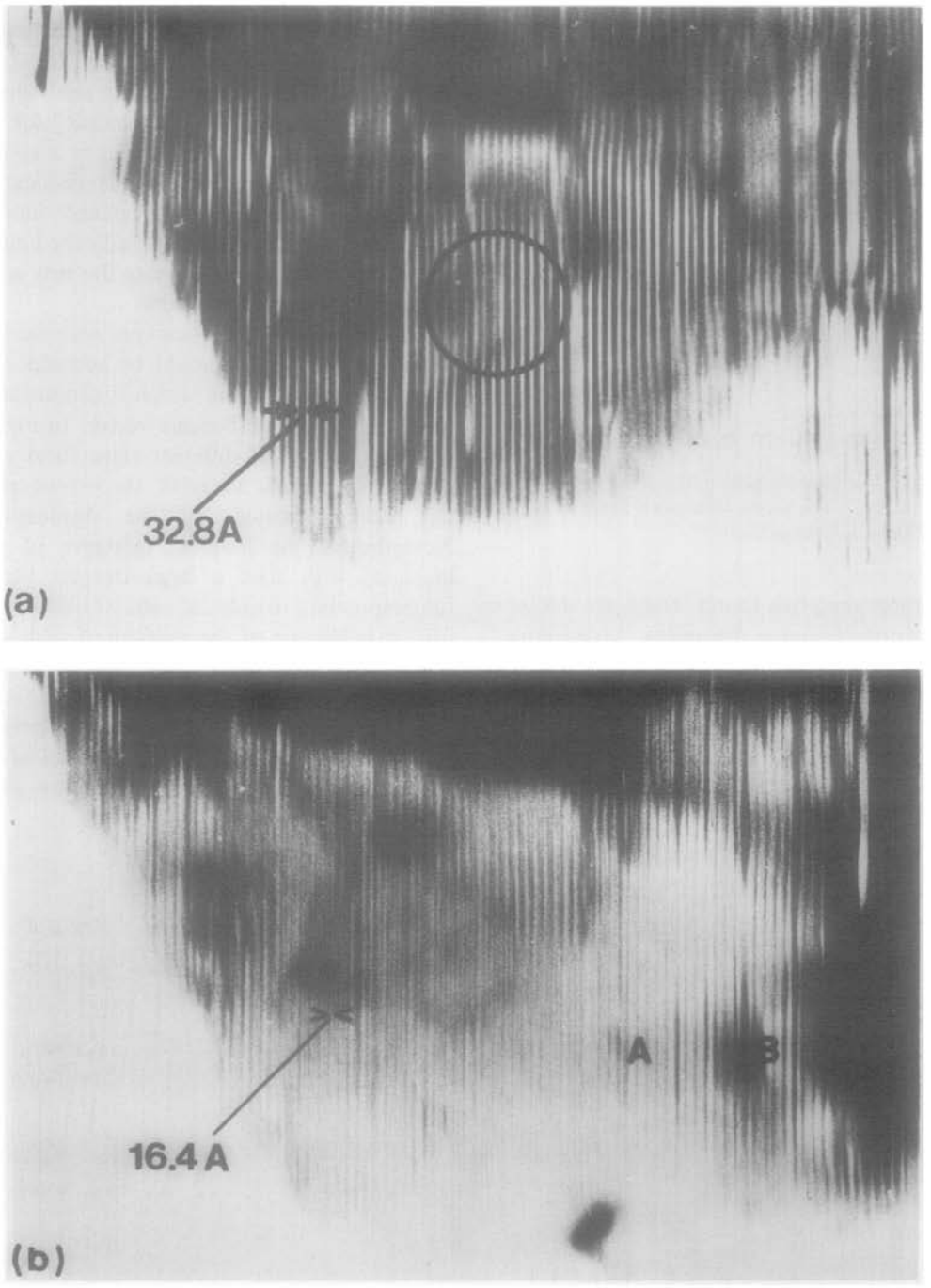


FIG. 10(a) Lattice image of the $W$ compound with dislocations. This corresponds to a double-width image taken with the (00.1), the (00.2), and the (00.0) reflections. (b) Lattice image of the same area as Fig. 10a taken by slightly tilting the beam incidence in order to avoid the double-width image due to double diffraction (00.1).

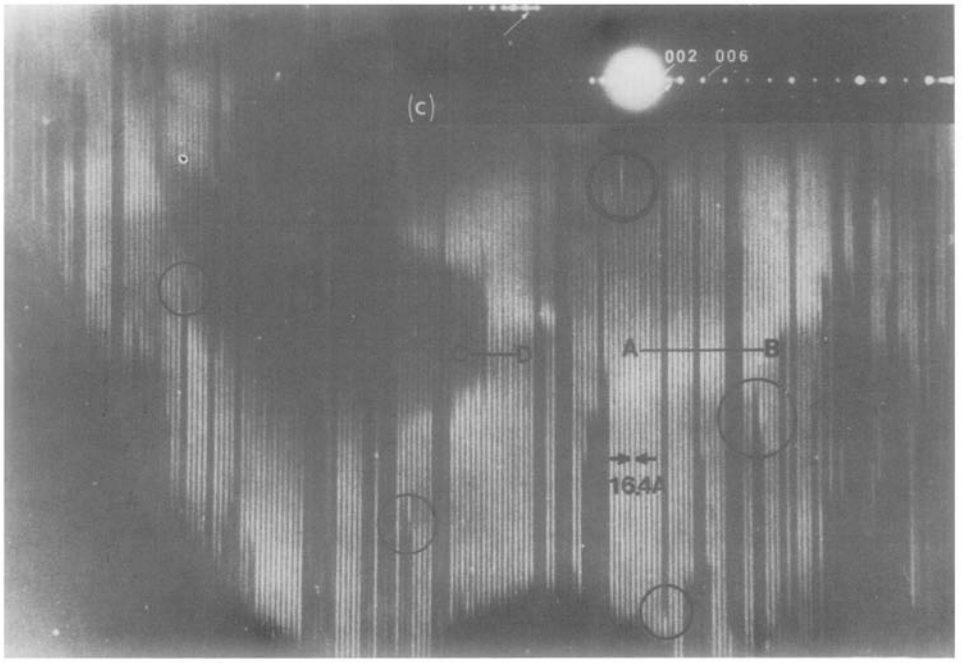


FIG. 10(c) Darkfield image of the same area, taken by using the spots (00.2) and (00.4) of the corresponding selected area diffraction pattern. Note the change in the contrast of the lattice image due to lattice distortion in circled areas. Arrows in the diffraction pattern indicate extra diffuse spots.

created by diffraction contrasts due to a lattice strain. However, this type of situation can be easily identified. An example is explained by a series of micrographs in Fig. 10. First, Fig. 10a shows the existence of several dislocations in the matrix of the *W* structure. The images of these dislocations are, however, double width images formed by double diffraction beams as is clear from the fact that the lattice period of the *W* structure appears as 32.8-Å stripe widths. That this is indirect information from other planes is also clear from the picture shown in Fig. 10b, which was taken under a different beam incidence condition in order to avoid the image formation by doubly diffracted beams. Here, the formation of 16.4-Å (00.2) fringes of the *W* structure and a smaller number of dislocation images compared to Fig. 10a are apparent. Thus, a comparison of images of the same area between A and B in both Figs. 10a and b clearly indicates that the double width images in (a) carry information of defects on other planes than the (00.1) plane. On the other hand, Fig. 10c shows a dark field lattice image utilizing reflections between the (00.2) and the (00.4) diffraction spots in the inset from the same area as (a) and (b). In Fig. 10c, on the other hand, many dark stripe contrasts with different widths from that of the *W* structure appear. A comparison of Fig. 10c with Fig. 10a thus indicates that these dark stripes are nothing but diffraction contrasts created by the strain field of defects or dislocations which have components of displacement vectors along the [00.1] direction. Further, in the encircled areas in Fig. 10c, fringe contrasts are found to change from black to white and vice versa due to the local changes of the displacement field.

That the extinction of the contrast in Fig. 10c is due to strain can also be shown by the measurement of the lattice period. In Fig. 11, a microdensitometer profile which is scanned along the line A–B in Fig. 10c is given. The positions $g_1$, $g_2$ and $h$ stripes correspond to the

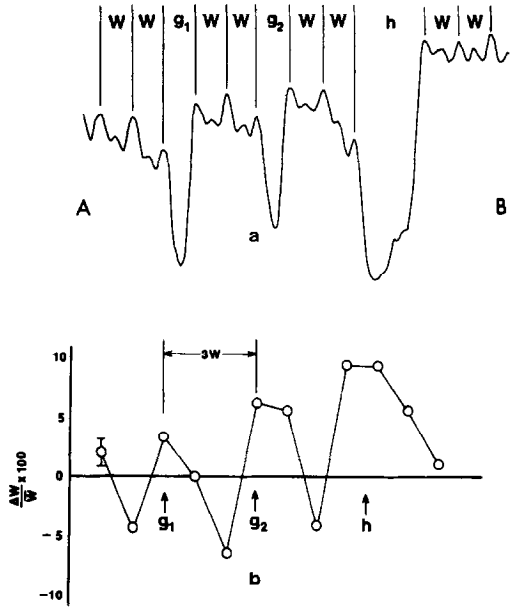


FIG. 11. (a) Microdensitometer profile along the line A–B in Fig. 10c. $g_1$, $g_2$, and $h$ correspond to the positions of the dark contrasts. (b) Variation of the spacing of the $W$ structure along the [00.1] direction.

widths of $W$ and $2W$, respectively, where $W$ approximates the unit cell period of the $W$ structure along the $c$ axis. However, a detailed measurement of these widths reveals a periodic change of the spacings. In Fig. 11, the deviation of the widths $\Delta W$ from the average value $\bar{W}$ of all the measured values of $W$ is plotted. The ordinary range of error involved in measuring $W$ is also indicated on the left-hand side of the figure. The quasi-periodic change of $W$ along the line A–B explains both the existence of the dark stripes as a diffraction contrast and the appearance of extra diffuse diffraction spots in the selected area diffraction pattern in the inset of Fig. 10c indicated by the arrows.

In Fig. 10c, the contrast of a dislocation is observed along the line C–D. Compare this image with the double width image of the same dislocation in the encircled area in Fig. 10a. In both cases, the interference contrast (lattice image) and the diffraction contrast (due to strain gradient) are clearly observed overlapped around the dislocation image. In Fig. 12, an enlarged image along the line C–D in Fig. 10c, a microdensitometer scan along the line C–D, and a schematic illustration of the image are shown. The stripe width $f$ in the microdensitometer scan is about 26 Å and corresponds to the period of the block $RSSS^*S^*$. A lattice model of the area shown on the right in Fig. 12 is obtained on the basis of this information. The Burgers vector of this dislocation corresponds to $\sim(6.7/33)\ c = 0.218c$, in which 6.7 Å corresponds to the size of the $R$ block while 33 Å corresponds to the unit cell size of the $W$ compound. From an energetical point of view, it is desirable that both the $SS^*$ and $R$ blocks be electrically neutral, as discussed earlier.

*Discussion*

The results of the present work on barium ferrite compounds in the composition range between the $M$ and the $W$ compound in the composition diagram (Fig. 2) show clearly that $M$, $X$, $W$, or $M_4S$ compounds intergrow in a microsyntactic fashion on the unit cell scale, creating structures of mixed periods. The feature is very similar to that found in Mg-doped $\beta$-alumina compounds reported earlier (*12*). Although quite peculiar, this characteristic is shared by many long period structures or those with polytypism like $V_nO_{2n-1}$ (*24*) and SiC (*3*, *25*). This intergrowth characteristic is an indication that many structures which exhibit different periods but with similar symmetry have almost equal stability and hence can coexist, provided that each unit cell of the series of compounds can be treated as a thermodynamically definable phase.

The interpretation of these lattice images which contain mixed period structures is, however, not straightforward. It is well known (*26*, *27*) that features of a lattice image are affected by such operation conditions as focusing, size of apertures, orientation, and thickness of specimens, and optical aberration constants of the electron microscope used. Although theoretical studies on lattice imaging concern-

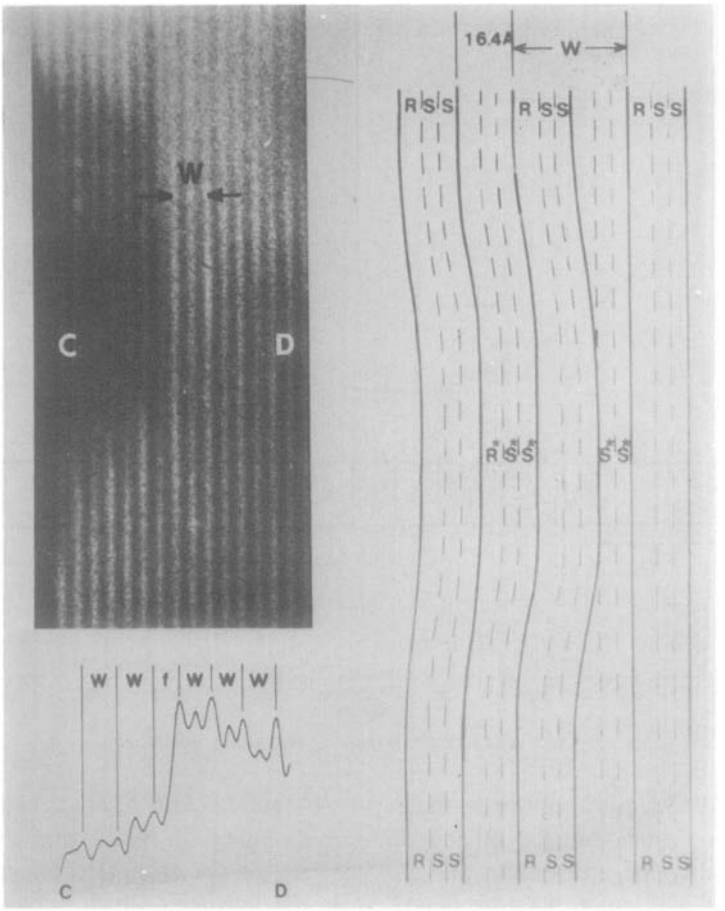


FIG. 12. (*Left*) Enlarged image of a dislocation which exists along the line *C–D* in Fig. 10c with the corresponding microdensitometer profile; *f* represents a defect fringe which corresponds to the dimension of the block *W–R*.
(*Right*) A possible structure of the dislocation.

ing perfectly periodic structures were carried out with success (*26–28*), little work on images of lattices with defects or with mixed period structures has been done. Therefore, if images are to be studied relative to lattice defects such as dislocations, stacking faults, or microsyntactic structures, a careful analysis of the images under varied conditions is necessary. In order to confirm the isolated existence of *R* and *S* blocks in this study, a one-dimensional lattice image calculation was made by assuming a plausible structural model with isolated *R* and *S* blocks in the *M* compound.

The basis for this image calculation was a giant cell model (*29*) in which several unit cell layers having defect structures among them were bounded by an empty margin at each side. A kinematical projected charge density approximation (*28*) was used for this calculation because the main aim of this calculation was to confirm qualitatively the appearance of isolated *R* and *S* blocks in the lattice image. The structure model taken and the calculated image intensity are shown in Fig. 13. Here, the giant unit cell period is chosen to be 20.5*M* (where *M* corresponds to the unit cell period of the hexagonal *M* compound with $RSR^*S^*$ stacking) in which three sets of 3*M* structures are connected by two kinds of faulted *M* structures represented

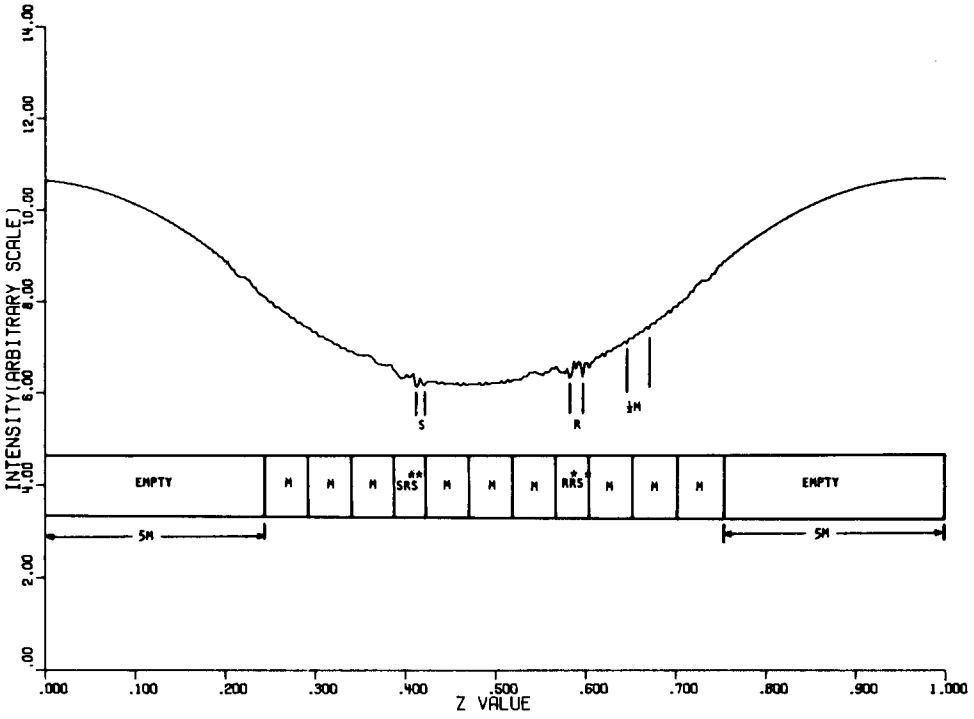


FIG. 13. Calculated lattice image of the structure model shown.

by $SR^*S^*$ and $RR^*S^*$. In other words, these faulted structures include isolated $R$ and $S$ blocks, respectively. The size of the margin was chosen as $5M$. The lattice image produced by the $(00.l)$ beams with $l$ up to $\pm 164$ was then calculated along the $c$-axis of the $M$ structure. The calculated curve corresponds to a condition of a certain degree of negative defocusing. Corresponding to the isolated $R$ and $S$ blocks in the model, fringes with widths which correspond to both the $S$ and $R$ blocks along with small fringes with widths which correspond to $(1/2)M$ appear. Therefore, the calculated image is found to reproduce the model qualitatively. Also, these features are in qualitative agreement with the real image (Fig. 7) which was taken by including nine strong beams (from the (00. − 8) to (00. + 8) $M$-reflections). In the calculated image, however, positional shifts of the $S$ and the $R$ blocks from the model and many small ripples and other interference fringes are seen. Also, in the real lattice image, fringe intensities of the $(1/2)M$ period (11.6 Å) are stronger than those corresponding to the $S$ and the $R$ blocks, contrary to the calculated image. In spite of such discrepancies which may be due to the crudeness of the model and to neglecting the effect of multiple scattering (calculation is applicable only to very thin crystals), it seems at least plausible that the lattice images actually observed in $\beta$-alumina and barium ferrites qualitatively represent the true situation in real crystals.

As was pointed out earlier, the intergrowth of many structures of different periods in a microsyntactic fashion indicates that these structures have practically the same stability. Because both the $\beta$-alumina type compounds and the Ba-ferrite type compounds are composed of two structural subunit blocks ($D$ and $S$ for $\beta$-alumina and $R$ and $S$ for Ba-ferrite) and because structures of different periods are simply stackings of different combinations of these two blocks, the appearance of these structures in a microsyntactic fashion indicates

that these subunit blocks are charge compensated individually or electrically neutral under these conditions. The isolated appearance of the $R$ and the $S$ blocks associated with the appearance of defects also supports the above concept.

On the other hand, it has been reasonably well established that, in Ba-ferrite (the $M$ compound), the $R$ block is negatively charged exactly by $-2e$ per unit cell while the $S$ block is positively charged exactly by $+2e$ (*14, 21*). It is, therefore, not clear that the charge distribution commonly adopted in the $M$ compound is compatible with the concept of the charge neutrality of individual subunit blocks even if the possibility of charge redistribution over the unit cell, which includes many subunit blocks, is taken into account. In addition, the situation concerning the charge compensation in $\beta$-alumina type compounds is still not quite understood in spite of extensive studies (*7–10*). Since this problem is closely connected to the "nonstoichiometry" of these compounds (*1*), further refinement of the structure of $\beta$-alumina seems necessary.

Here, it may be worth mentioning that the lattice fringes of structures with the rhombohedral symmetry like $X$ and $M_4S$ always appear in units of one third of their unit cell dimensions along the $c$-axis. These results simply mean that, for structures with rhombohedral symmetry, one third of the unit cell period along the $c$-axis is the physically meaningful unit for these structures. On the other hand, in the case of hexagonal structures like $M$ and $W$, the fringe size (a doublet) always corresponds to the size of the hexagonal unit cell.

## Acknowledgments

The authors wish to express their appreciation to Professor G. L. Liedl and Mr. Y. C. Tang for their cooperation during this work. Some of the work was done at the MRL laboratory of Northwestern University with their JEM–100 B electron microscope and the authors thank Professor M. Meshii of Northwestern University for his cooperation in placing the electron microscope at their disposal. One of the authors (Y.H.) would also like to thank the Sakkokai Fund for its financial support.

## References

1. H. Sato and Y. Hirotsu, *Mater. Res. Bull.* **11**, 1307 (1976).
2. D. J. M. Bevan, B. Hudson, and P. T. Moseley, *Mater. Res. Bull.* **9**, 1073 (1974).
3. H. Sato and S. Shinozaki, *Mater. Res. Bull.* **9**, 679 (1974).
4. M. Bettman and C. R. Peters, *J. Phys. Chem.* **73**, 1774 (1969).
5. M. Bettman and L. Terner, *Inorg. Chem.* **10**, 1442 (1971).
6. J. T. Kummer, "Progress in Solid State Chemistry", (J. O. McCaldin, Ed.), Vol. 7, p. 146, Pergamon, New York (1972).
7. C. R. Peters, M. Bettman, J. M. Moore, and M. P. Glick, *Acta Crystallogr. B***27**, 1826 (1971).
8. D. B. McWhan, S. J. Allen, Jr., J. P. Remeica, and P. D. Dernier, *Phys. Rev. Lett.* **35**, 953 (1975).
9. W. L. Roth, F. Reidinger, and S. LaPlaca, "Superionic Conductors" (G. D. Mahan and W. L. Roth, Eds.), p. 223, Plenum, New York (1975).
10. J. B. Boilot, G. Collin, R. Comes, J. Théry, R. Collongues, and A. Guinier, "Superionic Conductors" (G. D. Mathan and W. L. Roth, Eds.), p. 241, Plenum, New York (1976).
11. M. Bettman, *Mater. Res. Bull.* **10**, 229 (1975).
12. C. A. Beevers and M. A. S. Ross, *Z. Kristallogr.* **96**, 59 (1937).
13. V. Adelsköld, *Ark. Kemi, Mineral. Geol. A***12**, 1 (1938).
14. P. B. Braun, *Philips Res. Rep.* **12**, 491 (1957).
15. J. Smit and H. P. J. Wijn, "Ferrites," Wiley, New York (1959).
16. W. D. Townes, J. H. Fang, and A. J. Perrotta, *Z. Kristallogr.* **125**, 437 (1967).
17. J. Van Landuyt, S. Amelinckx, J. A. Kohn, and D. W. Eckart, *Mater. Res. Bull.* **18**, 1173 (1973).
18. J. Van Landuyt, S. Amelinckx, J. A. Kohn, and D. W. Eckart, *Solid State Chem.* **9**, 103 (1974).
19. J. S. Anderson and J. L. Hutchison, *Cont. Phys.* **16**, 443 (1975).
20. F. Haberey and M. Velicescu, *Acta Crystallogr. B***30**, 1597 (1974).
21. J. A. Kohn and D. W. Eckart, *Z. Krystallogr.* **119**, 454 (1964).
22. J. A. Kohn and D. W. Eckart, *Amer. Mineral.* **50**, 1371 (1965).
23. J. A. Kohn and D. W. Eckart, *J. Appl. Phys.* **35**, 968 (1965).

24. Y. HIROTSU, S. P. FAILE, AND H. SATO, to be published in *Mater. Res. Bull.* **13**, (1978).
25. S. SHINOZAKI, J. E. NOAKES, AND H. SATO, *J. Amer. Ceram. Soc.*, **61**, 237 (1978).
26. J. G. ALLPRESS AND J. V. SANDERS, *J. Appl. Crystallogr.* **6**, 165 (1973).
27. J. M. COWLEY AND S. IIJIMA, *Z. Naturforsch. A* **27**, 445 (1972).
28. G. R. AUSTIS, D. F. LYNCH, A. F. MOODIE, and M. A. O'KEEFE, *Acta Crystallogr. A*, **29**, 138 (1973).
29. D. A. JEFFERSON, G. R. MILLWARD, AND J. M. THOMAS, *Acta Crystallogr. A* **32**, 823 (1976).